

ICRR-Report-521-2005-4

KEK-TH-1035

STUPP-05-182

TUM-HEP-601/05

October 22, 2018

# Relic Abundance of LKP Dark Matter in UED model including Effects of Second KK Resonances

**Mitsuru Kakizaki<sup>a,b,1</sup>, Shigeki Matsumoto<sup>c,2</sup>, Yoshio Sato<sup>d,e,3</sup>**  
and **Masato Senami<sup>a,4</sup>**

<sup>a</sup>*ICRR, University of Tokyo, Kashiwa 277-8582, Japan*

<sup>b</sup>*Physikalisches Institut der Universität Bonn, Nussallee 12, 53115 Bonn, Germany*

<sup>c</sup>*Theory Group, KEK, Oho 1-1, Tsukuba, Ibaraki 305-0801, Japan*

<sup>d</sup>*Department of Physics, Saitama University, Saitama 338-8570, Japan*

<sup>e</sup>*Physik-Department, Technische Universität München,  
James-Frank-Strasse 85748 Garching, Germany*

## Abstract

We reevaluate the thermal relic density of the Kaluza-Klein (KK) dark matter in universal extra dimension models. In particular, we consider the effect of the resonance caused by second KK particles on the density. We find that the annihilation cross sections relevant to the density are significantly enhanced due to the resonance when the Higgs boson mass is large enough ( $m_h \gtrsim 200$  GeV). As a result, the mass of the dark matter particle consistent with the WMAP observation is increased compared to the result which does not include any resonance.

---

<sup>1</sup>kakizaki@th.physik.uni-bonn.de

<sup>2</sup>smatsu@post.kek.jp

<sup>3</sup>yoshio@krishna.th.phy.saitama-u.ac.jp

<sup>4</sup>senami@icrr.u-tokyo.ac.jp

## I. Introduction

Recent cosmological observations have determined the cosmological parameters precisely. In particular, the large difference between the mean density of the matter and the baryon has revealed that the large amount of non-baryonic cold dark matter exists in our universe [1]. The present interest concerning dark matter physics is its identification.

There are many discussions on the constituent of dark matter. Among those, weakly interacting massive particles (WIMPs) are excellent candidates for dark matter. They can explain not only the relic abundance of dark matter, but also the large scale structure of the present universe.

Many candidates for WIMPs have been proposed from models of particle physics. One of the most attractive WIMP candidates is the lightest supersymmetric particle (LSP) in supersymmetric (SUSY) extensions of the Standard Model (SM), and it has been extensively studied so far [2]. Recently an alternative candidate for WIMPs [3] has been proposed in universal extra dimension (UED) models [4], which are ones of well-motivated scenarios with TeV-scale extra dimensions [5].

UED models are natural extensions of SM to higher space-time dimensions. It is postulated that all particles in SM propagate in the compact spatial extra dimensions. From the four-dimensional point of view, the models are described as SM with extra particle contents, which are the towers of the Kaluza-Klein (KK) particles associated with each SM particle. The KK mass spectra are quantized due to the compactification, and labeled by KK number  $n$ . In the case of five-dimensional space-time the  $n$ -th KK particles have masses  $m^{(n)} \sim n/R$ , where  $R$  is the size of the extra dimension. Momentum conservation along with the compact extra dimension leads to the conservation of KK number.

The compactification is performed by an orbifold, which is required for reproducing the correct particle contents of SM. In other words, it is needed for obtaining chiral fermions at the zeroth KK level. The orbifolding violates the conservation of KK number and leaves its remnant called KK-parity conservation. Under the parity, particles at even (odd) KK levels have plus (minus) charge. As a result, the lightest first KK particle (LKP) is stabilized and is a viable candidate for WIMP dark matter. This situation is quite similar to conventional SUSY models, in which the LSP is stabilized by R-parity.

The LKP dark matter is frequently discussed [6]-[12], especially in the light of the

HEAT experiment, which reported larger positron fraction in the cosmic rays than its expectation [13]. The LKP has a possibility to account for the positron excess from its annihilation in the galactic halo [11]. On the other hand, it is difficult to explain the anomaly by annihilation of Majorana particles, such as LSP, due to the helicity suppression.

In this paper, we reevaluate the thermal abundance of the LKP dark matter in the minimal UED model: the simplest UED scenario which extra dimension is compactified on an  $S_1/Z_2$  orbifold. The first KK mode of photon,  $\gamma^{(1)}$ , is the LKP in the setup. The full calculation of the annihilation cross section at tree level relevant to the abundance has already been performed [6]. On the other hand, it was pointed out that one-loop diagrams in which second KK particles propagate in the  $s$ -channel significantly contribute to the cross sections [12]. Because the LKP dark matter is non-relativistic at the freeze-out temperature, the incident energy of two LKPs is almost equal to the masses of the second KK particles. The one-loop diagrams show the resonant behavior.

We perform the full calculation of the relic abundance including the effects of these resonances. In the preceding study, we briefly discussed the effect without considering the coannihilation processes [12]. On the other hand, as shown in Ref. [6], the coannihilation effects between the LKP and first KK particles of right-handed charged leptons significantly change the relic abundance of dark matter. Therefore it is worth evaluating how the relic abundance is affected by both the resonance and the coannihilation. In fact we will show the amazing result that the wide parameter region in the compactification scale,  $550 \text{ GeV} \lesssim 1/R \lesssim 770 \text{ GeV}$ , is consistent with the WMAP observation when the Higgs boson mass is large enough ( $m_h \gtrsim 200 \text{ GeV}$ ).

This paper is organized as follows. In the next section, we briefly review the minimal UED model. In particular, we focus on the mass spectra of KK particles. The annihilation cross sections including the effects of second KK resonances are discussed in Sec. III. Using the cross sections, we calculate the relic abundance of the LKP dark matter and evaluate the mass of dark matter consistent with the WMAP observation in Sec. IV. Section V is devoted to summary and discussion.

## II. Minimal UED model

The simplest UED model called the “minimal UED model” postulates one addi-

tional extra dimension, which is compactified on an  $S^1/Z_2$  orbifold. The compactification scale, the inverse of the size  $R$  of the extra dimension is constrained by the electroweak precision measurements as  $1/R \gtrsim 300$  GeV [4, 14].

The particle contents in the minimal UED is the same as those of SM. There are three gauge fields  $G, W, B$  and one Higgs doublet  $H$ . The matter contents are three generations of fermions: the quark doublets  $Q_i$ , the up- and down-type quark singlets  $U_i$  and  $D_i$ , the lepton doublets  $L_i$  and the charged lepton singlets  $E_i$ . The Latin index  $i$  runs over three generations. All these fields are defined on the five-dimensional space-time.

From the four-dimensional point of view, we have the usual SM particles and their KK modes with identical charges. Notice that all KK modes of the fermions are Dirac-type due to the vector property of a five-dimensional model. The interactions between these particles are completely determined by those of SM, and thus there is neither CP nor flavor problem in this model.

The UED model has some attractive features. One is the existence of a candidate particle for non-baryonic dark matter. Another is that the model is restrictive and has few number of undetermined parameters. There appear only two parameters related to new physics, the compactification scale  $1/R$  and the cutoff scale  $\Lambda$ , which is usually taken to be  $\Lambda R \sim \mathcal{O}(10)$  [4].

Although the masses of KK particles at each KK level are almost degenerate at tree level, radiative corrections relax the degeneracy [15]. Below we summarize radiatively corrected mass spectra related to our calculations.

As mentioned in the previous section, the LKP is identified with the first KK mode of photon in the minimal setup. The mass eigenstates and eigenvalues of the  $n$ -th KK photon,  $\gamma^{(n)}$ , and  $Z$  boson,  $Z^{(n)}$ , are obtained by diagonalizing the mass squared matrix in the  $(B^{(n)}, W^{3(n)})$  basis:

$$\begin{pmatrix} \frac{n^2}{R^2} + \delta m_{B^{(n)}}^2 + \frac{g'^2}{4}v^2 & \frac{g'g}{4}v^2 \\ \frac{g'g}{4}v^2 & \frac{n^2}{R^2} + \delta m_{W^{(n)}}^2 + \frac{g^2}{4}v^2 \end{pmatrix}, \quad (1)$$

where  $g$  ( $g'$ ) is the  $SU(2)_L$  ( $U(1)_Y$ ) gauge coupling constant, and  $v \simeq 246$  GeV is the vacuum expectation value of the Higgs field. The radiative corrections to the

massive KK gauge bosons are given by

$$\begin{aligned}\delta m_{B^{(n)}}^2 &= -\frac{39}{2} \frac{g'^2 \zeta(3)}{16\pi^4 R^2} - \frac{1}{6} \frac{g'^2 n^2}{16\pi^2 R^2} \ln(\Lambda^2 R^2) , \\ \delta m_{W^{(n)}}^2 &= -\frac{5}{2} \frac{g^2 \zeta(3)}{16\pi^4 R^2} + \frac{15}{2} \frac{g^2 n^2}{16\pi^2 R^2} \ln(\Lambda^2 R^2) .\end{aligned}\quad (2)$$

Given  $1/R \gg v$ ,  $\delta m_{W^{(n)}}^2 - \delta m_{B^{(n)}}^2$  exceeds the off-diagonal elements in Eq. (1). The weak mixing angles are extremely small for KK modes, and the LKP is dominantly composed of the first KK mode of the hypercharge gauge boson.

The LKP is highly degenerate with the first KK modes of right-handed charged leptons in mass even after including radiative corrections. The masses of the  $n$ -th KK lepton singlets are given by

$$m_{E^{(n)}} = \frac{n}{R} + \frac{9}{4} \frac{g'^2 n}{16\pi^2 R} \ln(\Lambda^2 R^2) , \quad (3)$$

where we ignore the mass terms induced by the electroweak symmetry breaking, because these terms are small enough compared to  $1/R$ . From the above equations, the degeneracy is found to be 1 % level.

Let us turn to a discussion on the mass of the second KK mode of the neutral and CP-even Higgs boson  $h^{(2)}$  in detail. This is because the mass difference between this KK Higgs and two LKPs plays an important role in the calculation of the annihilation cross sections (see the next section).

The mass of the neutral and CP-even Higgs boson is given by

$$m_{h^{(2)}}^2 = m_h^2 + \frac{4}{R^2} + \left( \frac{3}{2} g^2 + \frac{3}{4} g'^2 - \frac{m_h^2}{v^2} \right) \frac{4}{16\pi^2 R^2} \ln(\Lambda^2 R^2) , \quad (4)$$

where  $m_h$  is the mass of the SM Higgs boson. The last term comes from the radiative correction at one-loop level. In Fig. 1, we show the contour plots of the mass splitting between  $h^{(2)}$  and two  $\gamma^{(1)}$ s, which is defined as  $\delta \equiv (m_{h^{(2)}} - 2m_{\gamma^{(1)}})/2m_{\gamma^{(1)}}$ , in the  $(1/R, m_h)$  plane for  $\Lambda R = 20$  (a) and for  $\Lambda R = 50$  (b). These figures show that the degeneracy is  $\mathcal{O}(1)$  % level. One also finds region where the mass difference is almost zero.

### III. Annihilation cross sections including second KK resonances

In this section, we compute the annihilation cross sections including second KK resonances in the self-annihilation of LKP dark matter (i), the coannihilation

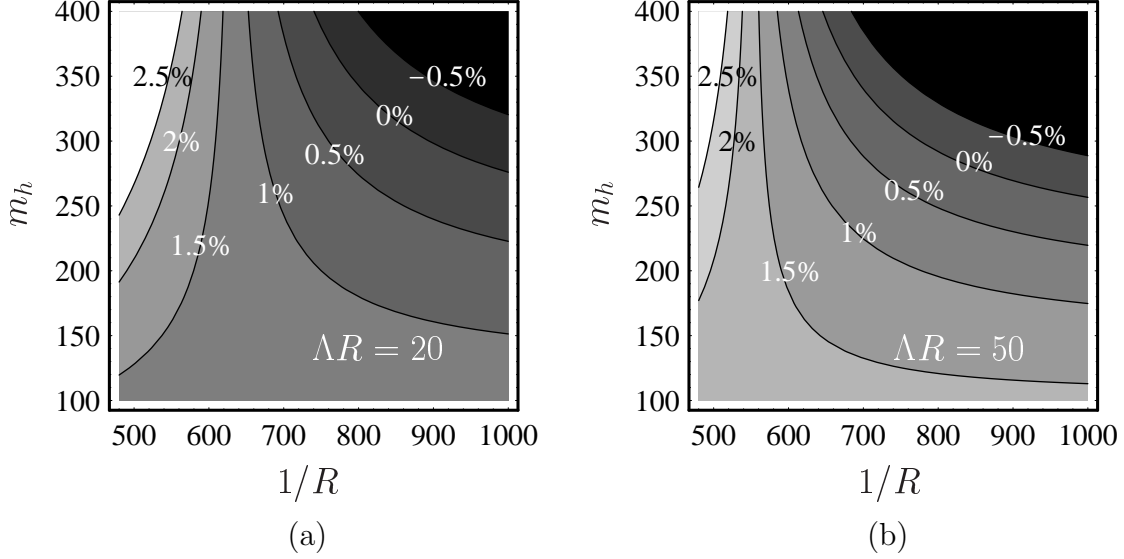


Figure 1: Contour plots of the mass splitting,  $\delta \equiv (m_{h^{(2)}} - 2m_{\gamma^{(1)}})/2m_{\gamma^{(1)}}$ , in the  $(1/R, m_h)$  plane for  $\Lambda R = 20$  (a) and for  $\Lambda R = 50$  (b).

cross sections for the LKP and the degenerate particles in mass (ii), and the self-annihilation cross sections of the coannihilating particles (iii). These cross sections are required for calculating the relic abundance of LKP dark matter.

#### (i) Self-annihilation of LKP dark matter ( $\gamma^{(1)}\gamma^{(1)} \rightarrow \text{SM particles}$ )

The calculation of the annihilation cross section at tree level have already been performed in Ref. [6]:

$$\sigma_{\text{Self}}^{(\text{Tree})} = \frac{95\pi\alpha_{\text{em}}^2}{81\cos^4\theta_W} \frac{5(2m^2 + s)L - 7s\beta}{s^2\beta^2} + \frac{\pi\alpha_{\text{em}}^2}{6\cos^4\theta_W s\beta}, \quad L \equiv \ln\left(\frac{1+\beta}{1-\beta}\right), \quad (5)$$

where  $\alpha_{\text{em}}$  is the fine structure constant,  $\theta_W$  is the weak mixing angle,  $m$  is the mass of the LKP,  $s$  is the center of mass energy squared,  $\beta$  is defined as  $\beta^2 \equiv 1 - 4m^2/s$ . In the calculation, we assume that all first KK modes have a equal mass and that all SM particles are massless.

At one-loop level, there is a diagram in which a second KK particle propagates in the  $s$ -channel. The diagram plays an important role in the annihilation process in the early universe. Since the incident particle is non-relativistic when its interactions are frozen out, the  $S$ -wave component in the initial state dominantly contributes to the process: the CP-even  $^1S_0$  and  $^5S_2$  states. Notice that the  $^3S_1$  state is forbidden due to the property of the neutral vector boson. Furthermore, the incident particle

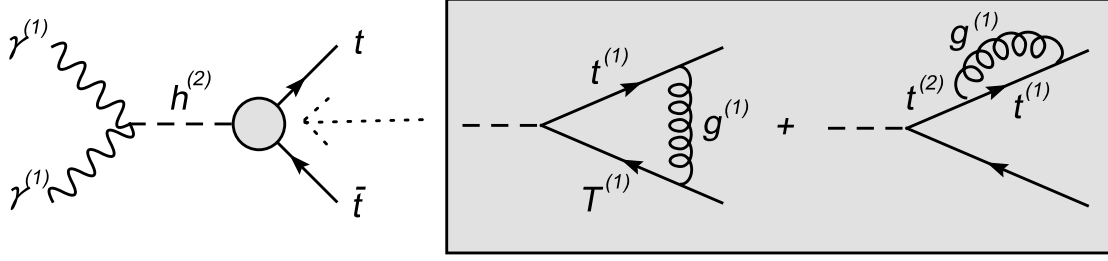


Figure 2: Resonant annihilation process of LKP dark matter through  $s$ -channel  $h^{(2)}$ . The dominant one-loop diagrams to the  $h^{(2)} - t - \bar{t}$  vertex stem from KK top quark–KK gluon mediation. Here  $t$  is the zero mode of the top quark, and  $t^{(n)}, T^{(n)}$  and  $g^{(n)}$  are the  $n$ -th KK modes of left- and right-handed top quarks and gluon respectively.

is electrically and color neutral. Therefore the contributing second KK particle is only the CP-even component of the second KK Higgs boson.

Although there is no transition from second KK states such as  $h^{(2)}$  into states involving only SM particles at tree level, their interactions appear through radiative corrections. Among those, the dominant interactions between  $h^{(2)}$  and SM particles come from the diagrams illustrated in Fig. 2 (right two diagrams). After performing loop integrals and taking leading logarithmic parts, we have the following effective interaction:

$$\mathcal{L}_{\text{eff}} = \frac{y_t \alpha_s}{12\pi} \ln(\Lambda^2 R^2) h^{(2)} \bar{t} t, \quad (6)$$

where  $y_t$  is the top Yukawa coupling constant and  $\alpha_s$  is the strong gauge coupling constant.

Let us discuss the decay width of the second KK Higgs particle, that is important for calculating the annihilation cross section with the resonance. The total decay width of  $h^{(2)}$  is governed by the decay mode into the top quarks through the one-loop diagrams in Fig. 2. In addition to the loop process, there are several modes at tree level: the decay modes into two first KK particles and those into one second KK particle and one SM particle. However, such tree-level processes are found to be forbidden or highly suppressed due to a kinematical reason or small Yukawa couplings. Therefore, the decay width of  $h^{(2)}$  is dominated by the one-loop process, and given by

$$\Gamma_{h^{(2)}} = \frac{y_t^2 \alpha_s^2 m_{h^{(2)}}}{384\pi^3} [\ln(\Lambda^2 R^2)]^2. \quad (7)$$

From the above effective interaction in Eq. (6) and the width in Eq. (7), we calculate the self-annihilation cross section including the effect of the  $h^{(2)}$  resonance

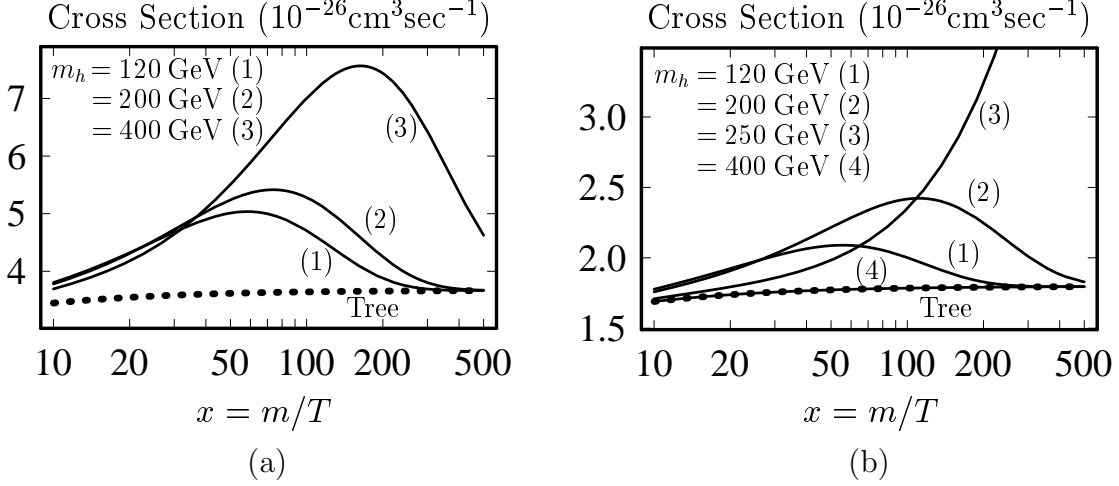


Figure 3: Thermally-averaged cross section as a function of the inverse of temperature  $x = m/T$ . Here we take  $1/R = 700$  GeV and  $\Lambda R = 20$  (a), and  $1/R = 1000$  GeV and  $\Lambda R = 50$  (b). In both Figs. (a) and (b), the dependence of the thermally-averaged cross section on the Higgs mass is shown. The dotted lines indicate the tree level results.

[12]:

$$\sigma_{\text{Self}} = \sigma_{\text{Self}}^{(\text{Tree})} + \sigma_{\text{Self}}^{(\text{Res})},$$

$$\sigma_{\text{Self}}^{(\text{Res})} = \frac{\pi \alpha_{\text{em}} \tan^2 \theta_W m_Z^2}{9m\beta} \frac{\Gamma_{h(2)}}{(s - m_{h(2)}^2)^2 + m_{h(2)}^2 \Gamma_{h(2)}^2} \left( 3 + \frac{s(s - 4m^2)}{4m^4} \right). \quad (8)$$

Here,  $\sigma_{\text{Self}}^{(\text{Tree})}$  is the tree-level result in Eq. (5), while  $\sigma_{\text{Self}}^{(\text{Res})}$  is obtained by calculating the one-loop diagrams shown in Fig. 2. Notice that the interferential contribution between the tree-level diagrams and the one-loop diagrams is negligible, because it suffers from the chirality suppression of the top quark mass. Since the incident energy approximates the second KK Higgs mass,  $s \simeq (2m)^2 \simeq m_{h(2)}^2$ , as emphasized in the previous sections, it is obvious that the resonant LKP dark matter annihilation is naturally realized.

The key quantity which controls the abundance is the thermally-averaged annihilation cross section defined as

$$\langle \sigma v \rangle_{\text{Self}} = 4\pi \left( \frac{m}{4\pi T} \right)^{3/2} \int_0^\infty dv v^2 (\sigma_{\text{Self}} v) \exp \left( -\frac{mv^2}{4T} \right), \quad (9)$$

where  $T$  is the temperature of the universe, and the relative velocity is given by  $v = 2\beta$ . At the rest of this paper, we use the notation  $\langle \cdots \rangle$  as a thermal average.

We numerically performed the integration and quantify the effect of the resonance on the annihilation process. In Fig. 3, we show the averaged cross section as a



function of the inverse of the temperature  $x = m/T$ . The left figure (a) shows the result for the case of  $1/R = 700$  GeV and  $\Lambda R = 20$ , and three solid lines correspond to  $m_h = 120$  GeV (1), 200 GeV (2) and 400 GeV (3). For  $m_h = 120$  GeV (1), the mass degeneracy between  $h^{(2)}$  and two  $\gamma^{(1)}$ s,  $\delta = (m_{h^{(2)}} - 2m_{\gamma^{(1)}})/2m_{\gamma^{(1)}}$ , is 1.25 %, and 1.11 % for  $m_h = 200$  GeV (2) and 0.41 % for  $m_h = 400$  GeV (3), respectively (see Fig.1). For comparison, the tree level calculation is also shown as a dotted line.

On the other hand, the right figure (b) is the result for  $1/R = 1000$  GeV and  $\Lambda R = 50$ , and four solid lines are  $m_h = 120$  GeV (1), 200 GeV (2), 250 GeV (3) and 400 GeV (4). The mass differences  $\delta$  are 1.45 % , 0.73 %, 0.10 % and  $-2.72$  % in these (1) to (4) cases.

The behavior and the magnitude of the thermally-averaged cross section considerably vary depending on the parameters. The annihilation cross section is enhanced due to the resonance compared to the tree-level result when the mass difference  $\delta$  is positive. Smaller  $\delta$  leads to larger enhancement at larger  $x$ . In particular,  $\delta$  is extremely small for the case (3) in the right figure, and the peak of the cross section is out of the range of the figure. In fact, the peak appears at  $x \sim 3000$  and the cross section is increased to  $10^{-25}\text{cm}^3\text{sec}^{-1}$ . On the contrary, for the result of negative  $\delta$  as in the case (4) in the right figure, the resonance enhancement does not occur and the tree-level cross section can be used for the calculation of the LKP abundance.

The enhancement of the cross section significantly contribute to the calculation of the abundance as we will explicitly see in the next section.

### (ii) Coannihilation ( $\gamma^{(1)}E_i^{(1)} \rightarrow \text{SM particles}$ )

Here, we discuss the coannihilation effects. The LKP,  $\gamma^{(1)}$ , is found to be highly degenerate with the first KK modes of the right-handed charged leptons,  $E_i^{(1)}$ , as stated in the previous section. It is thus indispensable to take the coannihilation processes between these particles into account in calculating the LKP dark matter abundance.

The coannihilation cross sections at tree level are also calculated in Ref. [6]:

$$\sigma_{\text{Co}}^{(\text{Tree})} = \frac{\pi\alpha_{\text{em}}^2}{\cos\theta_W^4} \frac{6L - \beta}{6\beta^2 s}, \quad (10)$$

where we assume that the mass of  $E_i^{(1)}$  is equal to that of  $\gamma^{(1)}$ .

At one-loop level there exist resonant processes in which the second KK modes of the right-handed charged leptons are exchanged in the  $s$ -channel, as shown in Fig. 4.

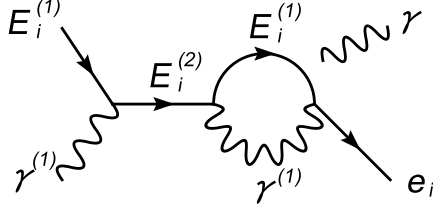


Figure 4: Resonant one-loop diagram which appears in the coannihilation process.

The  $E_i^{(2)}$ - $e_i$ - $\gamma$  vertex is given by dipole-type interaction, which does not suffer from ultra-violet divergence due to the gauge invariance. These coannihilation processes, however, are found to be negligible. The reason is as follows. The second KK mode of the right-handed charged lepton,  $E_i^{(2)}$ , dominantly decays into  $E_i^{(1)}$  and  $\gamma^{(1)}$  at tree level. Although the process is kinematically suppressed, it is still very large compared to the decay mode into  $e_i$  and  $\gamma$  at one-loop level. The branching ratio for the one-loop process is indeed less than 0.1 %. As a result, the one-loop diagram does not contribute to the coannihilation process. Therefore, we consider only the tree-level cross sections in the coannihilation processes.

(iii) Self-annihilation of coannihilating particles ( $E_i^{(1)} E_j^{(1)} \rightarrow \text{SM particles}$ )

Finally, we consider the self-annihilation processes for three generations of the first KK lepton singlets  $E_i^{(1)}$ , which are also important for calculating the LKP dark matter abundance. At tree level, the annihilation cross sections into SM particles are obtained as [6]

$$\begin{aligned}
& \sigma(E_i^{(1)} \bar{E}_i^{(1)}) \\
&= \frac{\pi \alpha_{\text{em}}^2}{12 \cos^4 \theta_W m^2} \frac{s\beta(12s^2 + 115m^2s + 68m^4) - 12L(2m^2s^2 - 5m^4s + 16m^6)}{s^3 \beta^2}, \\
& \sigma(E_i^{(1)} E_i^{(1)}) \\
&= \frac{\pi \alpha_{\text{em}}^2}{2 \cos^4 \theta_W m^2} \frac{s\beta(2s - m^2) + Lm^2(4s - 5m^2)}{s^2 \beta^2}, \tag{11}
\end{aligned}$$

for the same lepton flavor, and,

$$\begin{aligned}\sigma(E_i^{(1)} \bar{E}_j^{(1)}) &= \frac{\pi \alpha_{\text{em}}^2}{4 \cos^4 \theta_W m^2} \frac{\beta(4s + 9m^2) - 8Lm^2}{s\beta^2} , \\ \sigma(E_i^{(1)} E_j^{(1)}) &= \frac{\pi \alpha_{\text{em}}^2}{4 \cos^4 \theta_W m^2} \frac{4s - 3m^2}{s\beta} , \quad i \neq j,\end{aligned}\tag{12}$$

for different lepton flavor. One might expect that there appear many resonances via second KK particles in the  $\bar{E}_i^{(1)} E_i^{(1)}$  annihilation processes. However, this remark is not applicable to the minimal UED model. The reason is as follows. In the processes, the initial two-body state is electrically and color singlet, and  $E_i^{(1)}$  is singlet under the  $\text{SU}(2)_L$  gauge group. Furthermore only the  $S$ -wave state is relevant to non-relativistic annihilation. As a result, possible candidates for second KK particles causing resonant annihilation are the second KK mode of neutral pseudoscalar Higgs boson,  $A^{(2)}$ , and that of photon,  $\gamma^{(2)}$ . However both particles do not contribute to the annihilation cross section. The diagram in which  $A^{(2)}$  propagates in the  $s$ -channel is strongly suppressed due to the small Yukawa coupling. As for the  $\gamma^{(2)}$ -mediated process, the mass of  $\gamma^{(2)}$  is always smaller than twice the mass of  $E_i^{(1)}$ , avoiding any resonance. Since we can safely neglect any second KK resonance in these processes, the tree-level cross sections are sufficient for our calculation.

#### IV LKP dark matter abundance

We now evaluate the thermal relic abundance of the LKP dark matter using the annihilation cross sections obtained in the previous section and explore the parameter region of the model consistent with the WMAP observation. Since three generations of the next to LKPs,  $E_i^{(1)}$ , are highly degenerate with the LKP in mass, they are left over at the decoupling and decay after then. In this sense,  $E_i^{(1)}$  should be also recognized as dark matter particles in the early universe. Hence, the present density of dark matter is given by the sum of the number densities of the LKP and the next to LKPs.

The procedure for the calculation was developed in Ref. [16]. The time evolution of the total number density of dark matter,  $n \equiv n(\gamma^{(1)}) + \sum_i n(E_i^{(1)})$ , obeys the following Boltzmann equation:

$$\frac{dY}{dx} = -\frac{\langle \sigma v \rangle_{\text{eff}}}{Hx} s (Y^2 - Y_{\text{eq}}^2) , \quad Y_{\text{eq}} = 0.145 \frac{g_{\text{eff}}}{g_*} x^{3/2} e^{-x} , \tag{13}$$

where

$$g_{\text{eff}} = 3 + 12(1 + \Delta)^{3/2} e^{-x\Delta}, \quad \Delta = (m_{E^{(1)}} - m_{\gamma^{(1)}})/m_{\gamma^{(1)}}. \quad (14)$$

Here  $Y = n/s$  ( $Y_{\text{eq}} = n_{\text{eq}}/s$ ) describes the number density  $n$  ( $n_{\text{eq}}$ ) divided by the entropy density  $s$  of the universe, and  $x = m/T$  parametrizes the inverse of the temperature. The entropy density is given by  $s = 0.439 g_* m^3/x^3$ , with  $g_*$  being the number of relativistic degrees of freedom. The present entropy density is  $s_0 = 2900 \text{ cm}^{-3}$ . The Hubble parameter is  $H = 1.66 g_*^{1/2} m^2/x^2 m_{\text{Pl}}$ , where  $m_{\text{Pl}} = 1.22 \times 10^{19} \text{ GeV}$  is the Planck mass scale.

The effective cross section  $\sigma_{\text{eff}}$  involves not only the self-annihilation of LKP dark matters but also coannihilations, and given by

$$\begin{aligned} g_{\text{eff}}^2 \sigma_{\text{eff}} &= 9 \sigma_{\text{Self}} + 72(1 + \Delta)^{3/2} e^{-x\Delta} \sigma_{\text{Co}}^{(\text{Tree})} \\ &\quad + 24(1 + \Delta)^3 e^{-2x\Delta} \left[ \sigma \left( E_i^{(1)} E_i^{(1)} \right) + \sigma \left( E_i^{(1)} \bar{E}_i^{(1)} \right) \right] \\ &\quad + 48(1 + \Delta)^3 e^{-2x\Delta} \left[ \sigma \left( E_i^{(1)} E_j^{(1)} \right) + \sigma \left( E_i^{(1)} \bar{E}_j^{(1)} \right) \right], \quad i \neq j. \end{aligned} \quad (15)$$

As the mass of a coannihilating particle is heavy, the effect of the coannihilation on the relic abundance is exponentially suppressed.

By solving the Boltzmann equation in Eq. (13), we obtain the present abundance of dark matter  $Y_\infty$ . Since the non-relativistic LKP annihilation rate is enhanced by the resonance, numerical calculation is required in order to obtain reliable results [16]. It is useful to express the relic density in terms of  $\Omega h^2 = mn h^2/\rho_c$ , which is the ratio of the dark matter energy density to the critical density in the present universe,  $\rho_c = 1.1 \times 10^{-5} h^2 \text{ cm}^{-3}$ . The small letter  $h$  denotes the scaled Hubble parameter and takes a value  $h = 0.71_{-0.03}^{+0.04}$ .

It is instructive to observe a typical evolution of the abundance, which is shown in Fig. 5(a). In the early universe, the abundance is evolved on the line of the thermal equilibrium. After the interaction rate  $\Gamma = n \langle \sigma v \rangle_{\text{eff}}$  drops below the expansion rate  $H$  of the universe, the dark matter particles depart from the equilibrium. It is clear from Fig. 5(a) that the reactions are frozen out around  $T \sim m/25$ .

Generically, a present abundance is almost determined around the freeze-out temperature. However, the statement is not applicable to the case where the resonant annihilation occurs. After the freeze-out, the averaged annihilation cross section is significantly enhanced depending on temperature, as discussed in the previous section. The number density of dark matter particle gradually decreases due to the

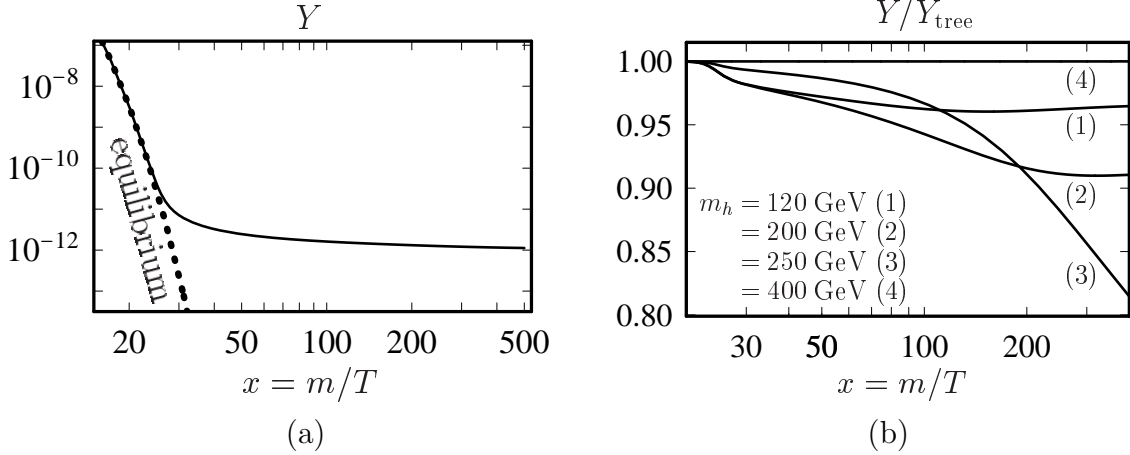


Figure 5: (a) Typical evolution of the abundance of LKP dark matter as a function of the temperature of the universe  $x = m/T$ . The dotted line indicates the abundance of the LKP at thermal equilibrium. (b) Ratio of the abundance  $Y$  including the effect of the second KK resonance to that at the tree level  $Y_{\text{tree}}$  after the freeze-out ( $20 < x < 400$ ). Here we take  $1/R = 1000$  GeV and  $\Lambda R = 50$ . Four lines correspond to the cases,  $m_h = 120$  GeV (1), 200 GeV (2), 250 GeV (3) and 400 GeV (4).

enhancement of the cross section, and eventually a smaller number of relics are left over, even if the abundance is large at the freeze-out temperature.

The phenomenon of the “late time decreasing” is clearly seen in Fig. 5(b). Here we plot the ratio of the abundance  $Y$  to that at the tree level  $Y_{\text{tree}}$  as a function of  $x = m/T$  after the freeze-out ( $20 < x < 400$ ). We set the compactification scale to be  $1/R = 1000$  GeV and the cutoff scale to be  $\Lambda R = 50$ . Four lines correspond to the cases when  $m_h = 120$  GeV (1), 200 GeV (2), 250 GeV (3) and 400 GeV (4). This figure demonstrates the decrease of the abundances due to the  $h^{(2)}$  pole. Especially for 250 GeV (3), the mass difference between two LKPs and the second KK Higgs boson is so tiny that the dark matter particles are found to be efficiently annihilated. (In the case of (3) the late time decreasing stops at  $x \sim 3000$ .)

In Fig. 6, the parameter region of the minimal UED model consistent with the WMAP observation is shown in the  $(1/R, m_h)$  plane. Black regions correspond to the  $1\sigma$  region of the relic abundance measured by WMAP ( $\Omega h^2 = 0.110 \pm 0.006$ ), and grey ones correspond to the  $2\sigma$  region. Here we take the cutoff scale to be  $\Lambda R = 20$  (Fig. 6(a)) and  $\Lambda R = 50$  (Fig. 6(b)). For comparison, tree-level results are also shown for  $\Lambda R = 20$  (Fig. 6(c)) and for  $\Lambda R = 50$  (Fig. 6(d)).

A comparison of Figs. 6(a) with (c) shows that the compactification scale  $1/R$  consistent with the observation is increased by 5 % due to the resonance. In the

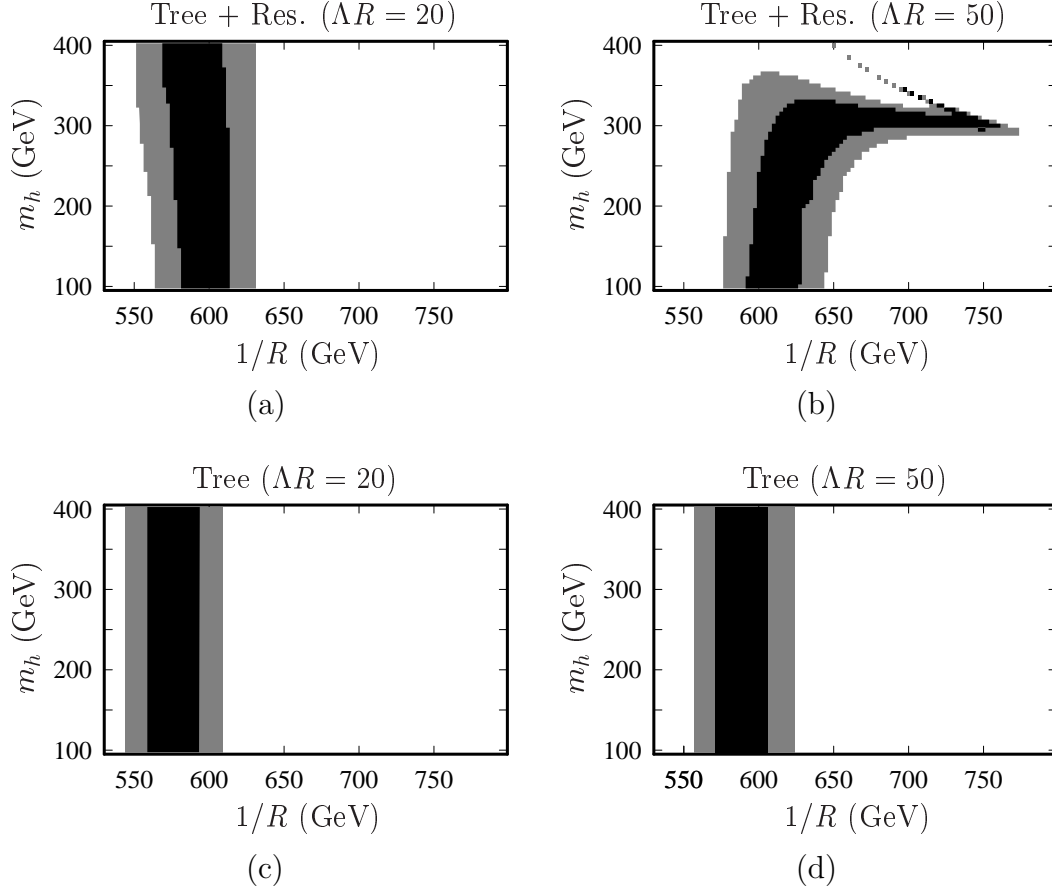


Figure 6: Parameter region of the minimal UED model consistent with the WMAP observation in the  $(1/R, m_h)$  plane for  $\Lambda R = 20$  (a) and for  $\Lambda R = 50$  (b). Black regions correspond to the  $1\sigma$  region of the relic abundance measured by WMAP ( $\Omega h^2 = 0.110 \pm 0.006$ ), and grey ones correspond to the  $2\sigma$  region. For comparison, tree-level results are also shown for  $\Lambda R = 20$  (c) and for  $\Lambda R = 50$  (d).

allowed region, the mass difference between the second KK Higgs and two LKPs is not so small, as seen in Fig. 1(a). Therefore, the resonance effect does not significantly alter the tree level result.

However, the resonance drastically changes the relic abundance when  $\Lambda R = 50$  as indicated in Figs. 6(b) and (d). The allowed region is strongly sensitive to the mass of the second KK Higgs, thus sensitive to the SM Higgs mass. For  $250 \text{ GeV} \lesssim m_h \lesssim 300 \text{ GeV}$ , due to the “late time decreasing” illustrated in Fig. 5(b), the allowed range of the compactification scale is extended to a higher mass scale, in sharp contrast to the preceding work [6]. On the contrary, for  $350 \text{ GeV} \lesssim m_h \lesssim 500 \text{ GeV}$ , the compactification scale is tightly constrained. Notice that the narrow region agrees with the degeneracy line ( $\delta = 0$ ) in Fig. 1(b). For  $m_h \gg 500 \text{ GeV}$ ,

the second KK Higgs mass is smaller than twice the LKP mass in the allowed region so that the resonance disappears: the region coincides with those obtained by the tree-level calculation.

## IV Summary and discussion

In this work, we have evaluated the thermal relic abundance of the LKP dark matter including not only the coannihilation but also the resonance in the minimal UED model. We have systematically investigated the effects of resonances on each annihilation process. We found that only the resonance with the second KK Higgs contributes to the abundance in the self-annihilation of LKP dark matters.

Furthermore, we have pointed out that the LKP dark matter abundance strongly depends on both the SM Higgs boson mass  $m_h$  and the cutoff scale  $\Lambda$  due to the resonance. A wider range of the compactification scale turns out to be consistent with cosmological observations. For example,  $580 \text{ GeV} \lesssim 1/R \lesssim 770 \text{ GeV}$  for  $m_h \simeq 300 \text{ GeV}$  and  $\Lambda R = 50$ . There also exist parameter region where the LKP mass is tightly constrained. The non-trivial dependence originates from the fact that the second KK Higgs mass plays a crucial role in determining the relic dark matter abundance due to the resonant annihilation.

## Acknowledgments

The work of M.K. is supported in part by the Japan Society for the Promotion of Science.

## References

- [1] C. L. Bennett *et al.*, *Astrophys. J. Suppl.* **148** (2003) 1; D. N. Spergel *et al.* [WMAP Collaboration], *Astrophys. J. Suppl.* **148** (2003) 175.
- [2] For reviews, see for instance, G. Jungman, M. Kamionkowski and K. Griest, *Phys. Rept.* **267** (1996) 195; L. Bergstrom, *Rept. Prog. Phys.* **63** (2000) 793; C. Munoz, *Int. J. Mod. Phys. A* **19** (2004) 3093; G. Bertone, D. Hooper and J. Silk, *Phys. Rept.* **405** (2005) 279.

- [3] E. W. Kolb and R. Slansky, Phys. Lett. B **135** (1984) 378; K. R. Dienes, E. Dudas and T. Gherghetta, Nucl. Phys. B **537** (1999) 47.
- [4] T. Appelquist, H. C. Cheng and B. A. Dobrescu, Phys. Rev. D **64** (2001) 035002.
- [5] I. Antoniadis, Phys. Lett. B **246** (1990) 377; N. Arkani-Hamed, S. Dimopoulos and G. R. Dvali, Phys. Lett. B **429** (1998) 263.
- [6] G. Servant and T. M. P. Tait, Nucl. Phys. B **650** (2003) 391.
- [7] H. C. Cheng, J. L. Feng and K. T. Matchev, Phys. Rev. Lett. **89** (2002) 211301.
- [8] G. Servant and T. M. P. Tait, New J. Phys. **4** (2002) 99; D. Majumdar, Phys. Rev. D **67** (2003) 095010.
- [9] D. Hooper and G. D. Kribs, Phys. Rev. D **67** (2003) 055003; G. Bertone, G. Servant and G. Sigl, Phys. Rev. D **68** (2003) 044008; L. Bergstrom, T. Bringmann, M. Eriksson and M. Gustafsson, Phys. Rev. Lett. **94** (2005) 131301; E. A. Baltz and D. Hooper, JCAP **0507** (2005) 001.
- [10] L. Bergstrom, T. Bringmann, M. Eriksson and M. Gustafsson, JCAP **0504** (2005) 004.
- [11] D. Hooper and G. D. Kribs, Phys. Rev. D **70** (2004) 115004; D. Hooper and J. Silk, Phys. Rev. D **71** (2005) 083503.
- [12] M. Kakizaki, S. Matsumoto, Y. Sato and M. Senami, Phys. Rev. D **71** (2005) 123522.
- [13] S. W. Barwick *et al.* [HEAT Collaboration], Astrophys. J. **482** (1997) L191; S. Coutu *et al.*, Astropart. Phys. **11** (1999) 429; J. J. Beatty *et al.*, Phys. Rev. Lett. **93** (2004) 241102.
- [14] K. Agashe, N. G. Deshpande and G. H. Wu, Phys. Lett. B **511** (2001) 85; K. Agashe, N. G. Deshpande and G. H. Wu, Phys. Lett. B **514** (2001) 309; T. Appelquist and B. A. Dobrescu, Phys. Lett. B **516** (2001) 85; F. J. Petriello, JHEP **0205** (2002) 003; T. Appelquist and H. U. Yee, Phys. Rev. D **67** (2003) 055002; D. Chakraverty, K. Huitu and A. Kundu, Phys. Lett. B **558** (2003) 173; A. J. Buras, M. Spranger and A. Weiler, Nucl. Phys. B **660** (2003) 225; J. F. Oliver, J. Papavassiliou and A. Santamaria, Phys. Rev. D **67** (2003) 056002.
- [15] H. C. Cheng, K. T. Matchev and M. Schmaltz, Phys. Rev. D **66** (2002) 036005.
- [16] K. Griest and D. Seckel, Phys. Rev. D **43** (1991) 3191.